J. Nonlinear Sci. Vol. 1: pp. 289–311 (1991)

Journal of Nonlinear Science

Analysis of Stable Two-Dimensional Patterns in Contractile Cytogel

M. A. Lewis[1,2] and J. D. Murray[1]

[1] Department of Applied Mathematics, FS–20 and
[2] Department of Zoology, NJ–15, University of Washington, Seattle, WA 98195, USA

Received May 1, 1991; accepted for publication July 17, 1991
Communicated by Stephen Wiggins

Summary. Contractile actomyosin systems play a central role in the generation of intracellular patterns. Models for pattern formation have benefited greatly from the application of mechanochemical theory. However, investigations of the patterns have been primarily qualitative in nature; the two-dimensional nature of the evolving patterns has not yet been addressed mathematically, nor has the evolution of stable heterogeneous steady-state solutions. We consider these issues, supporting our analytical predictions with numerical simulations in one and two spatial dimensions. We show how, for certain gels, the two and three-dimensional tensor equation which describes a balance of forces can be reduced to a reaction-diffusion equation.

Key words. cytogel, mechanochemical, two-dimensional patterns, cellular differentiation, pattern formation, stability.

1. Introduction

Eucaryotic cells (those with nuclei) are highly organized and differentiated. They are capable of altering their shape, repositioning their organelles (or internal structures) and, in many cases, moving from one place to another. These properties of shape, internal organization and movement depend on the cytoskeleton, or a complex network of protein filaments in the cytoplasm (Alberts et al., 1983). Within the cytoskeleton, a contractile actomyosin gel provides the basis for generating forces.

The relationship between the molecular structure of the cytoplasm and its mechanical properties is the key in the understanding of cytoplasmic operation. Current theory points to a sol-gel phase change as the crucial feature governing contractile activity (Taylor et al., 1979; Condeelis, 1983). This theory has been successfully incorporated into mechanochemical models for sol-gel dynamics which have been applied to subjects as diverse as the formation of hexagonal microvilli patterns (Oster et al., 1985), amoeboid movement (Oster, 1984) and plasmodial oscillations in *Physarium*

(Oster and Odell, 1984). Such models use a system of partial differential equations to describe quantitatively the sol-gel chemical kinetics and stress-strain mechanical relationships within an element of cytogel. Investigations have been primarily qualitative in nature; the two-dimensional nature of the evolving patterns has not yet been addressed mathematically, nor has the evolution of stable heterogeneous steady state solutions. This analysis is, however, essential for a full understanding of the long-term pattern formation potential of mechanochemical sol-gel models. The fact that contractile actomyosin systems play a central role in the generation of intracellular forces for movement and pattern formation is justification for a detailed analysis.

In this paper we consider a slightly modified version of the Oster et al. (1985) model for microvilli pattern formation (see Lewis, 1990). Our model has a wider application in the context of pattern formation in the cortex of *Paramecium* (Lewis, 1990) and possibly can explain a mechanism for the generation of hair cell patterns in the inner ear (Oster et al., 1985). It is assumed that, within the cell, mechanisms adhere to Newtonian dynamics. At the intracellular level inertial terms are negligible compared to viscous and elastic forces; motions cease as soon as the forces are turned off (see, for example, Purcell, 1977). Thus the cytogel system is described by two equations, the first of which reflects the fact that, at any given time, the mechanical forces acting upon the cytogel must balance while the second describes the chemical dynamics for the gel. The model is

$$\nabla \cdot (\boldsymbol{\sigma}_V + \boldsymbol{\sigma}_E + \boldsymbol{\sigma}_A + \boldsymbol{\sigma}_{OS}) = \mathbf{0}, \tag{1}$$

$$\frac{\partial G}{\partial t} + \nabla \cdot \left(G \frac{\partial \mathbf{u}}{\partial t} \right) - D_G \Delta G - k_+(\theta) S_0 + k_-(\theta) G = 0, \tag{2}$$

where G is the concentration of gel, S_0 is a constant sol concentration, D_G is a diffusion coefficient for the gel, $\mathbf{u}$ is a vector denoting the displacement of the stable elements (noncontractile microtubules and intermediate filaments) from their original unstrained position, and $\theta = \nabla \cdot \mathbf{u}$ is the dilation. The dilation-dependent conversion rates from gel to sol ($k_+(\theta)$) and from sol to gel ($k_-(\theta)$) are shown qualitatively in Figure 1. The viscous, elastic, active traction, and osmotic stress components of (1)

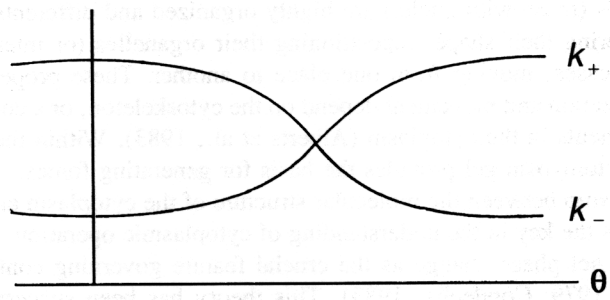

Fig. 1. The sol-gel dynamics as a function of dilation. The gelation rate (k_+) and solation rate (k_-) are given as qualitative functions of the dilation, θ.

are given by

$$\boldsymbol{\sigma}_v = \frac{G}{c_0}(\mu_1 \epsilon_t + \mu_2 \theta_t \mathbf{I}), \tag{3}$$

$$\boldsymbol{\sigma}_E = \gamma \frac{G}{c_0}[\boldsymbol{\epsilon} - \beta \Delta \boldsymbol{\epsilon} + \hat{\nu}(\theta - \beta \Delta \theta)\mathbf{I}], \tag{4}$$

$$\boldsymbol{\sigma}_A = \frac{G}{c_0}\tau(\theta)\mathbf{I}, \tag{5}$$

$$\boldsymbol{\sigma}_{OS} = -\pi(\theta)\mathbf{I}, \tag{6}$$

where $\boldsymbol{\epsilon} = \frac{1}{2}(\nabla \mathbf{u} + \mathbf{u}\nabla)$ is the strain tensor, c_0 is the density of cytogel at $\theta = 0$, μ_1 and μ_2 are the shear and bulk viscosities of the gel, respectively, $\gamma = E/(1 + \nu)$ and $\hat{\nu} = \nu/(1 - 2\nu)$ are given in terms of the Young's modulus (E) and the Poisson ratio (ν), and $\beta > 0$ is a measure of long-range elastic effects. The dilation-dependent traction ($\tau(\theta)$) and osmotic stress ($\pi(\theta)$) terms are shown qualitatively in Figure 2. The reader is referred to Oster et al. (1985) and Lewis (1990) for a detailed derivation of the model (1)–(2).

Under the assumption of a time-independent boundary stress σ_0 the force balance equation (1) can be integrated in one dimension to give a pair of reaction-diffusion-

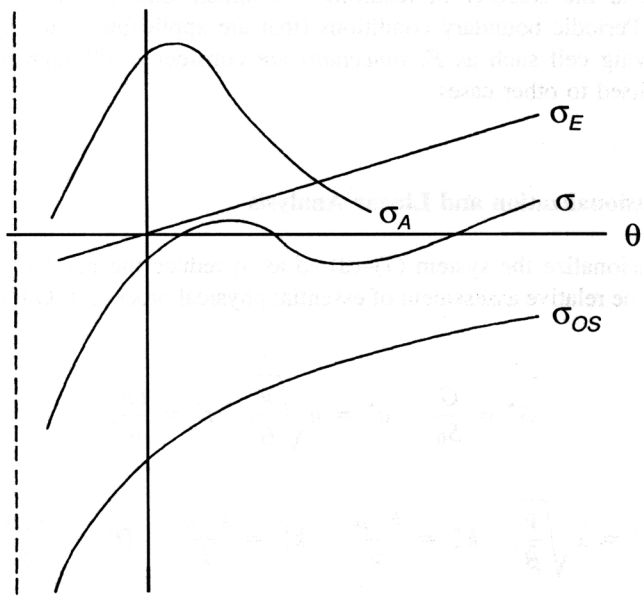

Fig. 2. Stress-strain relationship for actin gel. Ignoring sol-gel dynamics, the relationship is shown for a constant gel concentration.

convection equations, namely

$$\mu \frac{G}{c_0}\frac{\partial \theta}{\partial t} - \tilde{\beta}\frac{G}{c_0}\frac{\partial^2 \theta}{\partial x^2} + \tilde{\nu}\frac{G}{c_0}G\theta + \frac{G}{c_0}\tau(\theta) - \pi(\theta) + \sigma_0 = 0, \tag{7}$$

$$\frac{\partial G}{\partial t} + \frac{\partial}{\partial x}\left(G\frac{\partial u}{\partial t}\right) - D_G\frac{\partial^2 G}{\partial x^2} - k_+(\theta)S_0 + k_-(\theta)G = 0, \tag{8}$$

where $\mu = \mu_1 + \mu_2$, $\tilde{\nu} = \gamma(1 + \hat{\nu})$, and $\tilde{\beta} = \tilde{\nu}\beta$.

The dilation (θ) plays the role of *reactant* in (7). Reaction-diffusion systems of this form have been widely studied and, given appropriate dynamics, are known to yield spatial patterns (see, for example, Murray, 1989) although a convection term, such as the one in (8), is usually not present. Linear analysis (reviewed in Section 2) about the homogeneous steady state solution indicates that this system exhibits instabilities with a wave number k_c when the diffusion coefficient for the gel (D_G) exceeds a critical value (Lewis, 1990; see also Oster et al., 1985). In Section 3 we show that, over a long time scale, the growth of linear instabilities is bounded by nonlinear terms to yield a stable stationary steady state solution. Through numerical simulation of the resulting patterns, we show how the analytical theory predicts their evolution. Section 4 considers the stationary pattern formation potential that the cytogel model [(1)–(2)] exhibits in two spatial dimensions through a two-dimensional analysis of the linear behavior of small perturbations away from the steady state. We show how, for certain gels, the two-dimensional tensor equation which describes the force balance (1) can be reduced to a reaction-diffusion equation. The full nonlinear system is solved numerically and the stability of resulting two-dimensional patterns is numerically investigated. Periodic boundary conditions (that are applicable to the cytogel cortex of a free-moving cell such as *Paramecium*) are considered although results can be easily generalised to other cases.

2. Nondimensionalization and Linear Analysis

We nondimensionalize the system (7)–(8) so as to reduce the number of parameters and facilitate the relative assessment of essential physical processes. Our new variables are

$$G^* = \frac{G}{S_0}, \quad u^* = u\sqrt{\frac{\tilde{\nu}}{\tilde{\beta}}}, \quad t^* = \frac{t\tilde{\nu}}{\mu},$$

$$x^* = x\sqrt{\frac{\tilde{\nu}}{\tilde{\beta}}}, \quad k_+^* = \frac{k_+\mu}{\tilde{\nu}}, \quad k_-^* = \frac{k_-\mu}{\tilde{\nu}}, \quad D^* = \frac{D_G\mu}{\tilde{\beta}},$$

$$\tau^* = \frac{\tau}{\tilde{\nu}}, \quad \pi^* = \frac{\pi c_0}{S_0\tilde{\nu}}, \quad \sigma_0^* = \frac{\sigma_0 c_0}{S_0\tilde{\nu}}.$$

Substituting these quantities into (7)–(8), and dropping the asterisks for notational simplicity, we obtain

$$G\frac{\partial\theta}{\partial t} - G\frac{\partial^2\theta}{\partial x^2} - \Phi(G,\theta) = 0, \tag{9}$$

$$\frac{\partial G}{\partial t} + \frac{\partial}{\partial x}\left(G\frac{\partial u}{\partial t}\right) - D\frac{\partial^2 G}{\partial x^2} - \Gamma(G,\theta) = 0, \tag{10}$$

where

$$\Phi(G,\theta) = -G\theta - G\tau(\theta) + \pi(\theta) - \sigma_0, \tag{11}$$

$$\Gamma(G,\theta) = k_+(\theta) - k_-(\theta)G. \tag{12}$$

We consider the behavior of small perturbations of the state variables away from their steady state,

$$(G_0,\theta_0) = \left(\frac{k_+(\theta_0)}{k_-(\theta_0)},\theta_0\right), \tag{13}$$

where θ_0 is the solution to

$$k_+(\theta_0)[\theta_0 + \tau(\theta_0)]/k_-(\theta_0) - \pi(\theta_0) + \sigma_0 = 0.$$

Linearization of (9)–(10) gives rise to a homogeneous system of linear equations describing the behavior of these small disturbances. This system yields a dispersion relation between the temporal and spatial components of the perturbations to the parameters in the model, thereby determining when and how the steady state can become linearly unstable.

The linearized form of (9)–(10) is

$$\begin{pmatrix} G_0\left(\frac{\partial}{\partial t} - \frac{\partial^2}{\partial x^2}\right) - \Phi_\theta & -\Phi_G \\ G_0\frac{\partial}{\partial t} - \Gamma_\theta & \frac{\partial}{\partial t} - D\frac{\partial^2}{\partial x^2} - \Gamma_G \end{pmatrix}\begin{pmatrix} \theta - \theta_0 \\ G - G_0 \end{pmatrix} = \mathbf{0}, \tag{14}$$

where

$$\Phi_\theta = \frac{\partial\Phi}{\partial\theta}(G_0,\theta_0), \qquad \Phi_G = \frac{\partial\Phi}{\partial G}(G_0,\theta_0),$$

$$\Gamma_\theta = \frac{\partial\Gamma}{\partial\theta}(G_0,\theta_0), \qquad \Gamma_G = \frac{\partial\Gamma}{\partial G}(G_0,\theta_0).$$

We use the principle of superposition and assume

$$\theta - \theta_0,\ G - G_0 \propto \exp(\sigma t + ikx). \tag{15}$$

Substitution into (14) gives a dispersion relation between σ and k^2 that must be

satisfied for nontrivial solutions. This is

$$G_0\sigma^2 + b(k^2)\sigma + c(k^2) = 0, \tag{16}$$

where

$$b(k^2) = \Phi_G G_0 - \Gamma_G G_0 - \Phi_\theta + G_0(1 + D)k^2, \tag{17}$$

$$c(k^2) = \Gamma_G\Phi_\theta - \Phi_G\Gamma_\theta - (D\Phi_\theta + G_0\Gamma_G)k^2 + G_0Dk^4. \tag{18}$$

For the uniform steady state to be stable to perturbations with a spatial component, we require that the roots of (16) have a negative real part for all positive k^2. If there is a root with a positive real part for some k^2, then the linear theory predicts that small random perturbations away from the steady state will grow exponentially with a spatial wavelength of $2\pi/k$.

2.1 Conditions for Bifurcation to Spatial Pattern

Necessary and sufficient conditions for the roots of (16) to have negative real parts are

$$b(k^2) > 0 \quad \text{and} \quad c(k^2) > 0 \tag{19}$$

for all positive k^2. To ensure that spatial pattern bifurcations have finite wave numbers k, where $0 < k^2 < \infty$, we must meet (19) for very large and very small k^2. Because $G_0 > 0$ and $D > 0$, the criterion (19) is satisfied as $k^2 \to \infty$. For (19) to be satisfied as $k^2 \to 0^+$, we require that

$$b(0) = \Phi_G G_0 - \Gamma_G G_0 - \Phi_\theta > 0, \tag{20}$$

$$c(0) = \Gamma_G\Phi_\theta - \Phi_G\Gamma_\theta > 0. \tag{21}$$

The first condition in (19) is always met by (20) as $b(k^2) \geq b(0)$. However, violation of the second condition in (19) results in a $\sigma = 0$ root for (16). This leads to a bifurcation to the exponential growth of unstable stationary modes.

We consider the case where a bifurcation to linear instability occurs for a critical wave number k_c as an eigenvalue of the linear system passes through zero. In terms of the stability criterion (19), the bifurcation point is given by $b(k^2) > 0$ for all k and

$$c(k^2)\begin{cases} = 0, & \text{if } k = k_c \\ > 0, & \text{if } k \neq k_c. \end{cases}$$

The minimum for $c(k^2)$ is found when

$$2G_0Dk^2 - D\Phi_\theta - G_0\Gamma_G = 0. \tag{22}$$

Thus we require that

$$D\Phi_\theta + G_0\Gamma_G > 0. \tag{23}$$

We define the critical diffusion value D_c as the value of D which yields a critical sign change for the maximum root of (16). This bifurcation occurs when the minimum for $c(k^2)$ passes through zero. Thus $D = D_c$ satisfies

$$(D\Phi_\theta - G_0\Gamma_G)^2 + 4G_0D\Phi_G\Gamma_\theta = 0 \tag{24}$$

and the corresponding critical wave number k_c is given by (22) as

$$k_c^2 = (D_c\Phi_\theta + G_0\Gamma_G)/(2G_0D_c). \tag{25}$$

Given the qualitative forms of $k_+(\theta)$ and $k_-(\theta)$ (Figure 1), the constraints (20), (21), and (23) require that $\Phi_\theta > 0$ and $\Phi_G < 0$. This is typically the case when $\sigma_0 < 0$. We choose D_c as the largest root of (24) so as to meet the constraint (23). Thus, as D increases through D_c, the maximum root for (16) passes through zero and linear analysis (15) predicts a corresponding bifurcation to the growth of unstable, stationary modes with wave number k_c.

3. Nonlinear Analysis

In this section we analyze the nonlinear behavior of exponentially growing stationary modes, predicted by linear analysis (Section 2) as occurring when the maximum eigenvalue for (16) increases through zero. Provided that (20), (21), and (23) are met, this bifurcation to linearly unstable modes takes place as D increases through D_c, the larger root of (24). The resulting wavelength of the growing pattern is $2\pi/k_c$, where k_c is given by (25). Using standard nonlinear methods, we derive a Landau equation for the amplitude of these perturbations and show that they grow until nonlinear terms bound the linear growth terms. This results in the evolution of stationary spatial patterns.

We make an ε^2 perturbation away from the critical value for D,

$$D = D_c + \varepsilon^2\nu, \quad \text{where} \quad 0 < \varepsilon \ll 1 \quad \text{and} \quad \nu = \pm 1, \tag{26}$$

and use this as the basis for a series expansion of σ,

$$\sigma(k_c^2, D) = \sigma(k_c^2, D_c) + \frac{\partial\sigma}{\partial D}(k_c^2, D_c)\,\varepsilon^2\nu + \mathcal{O}(\varepsilon^4). \tag{27}$$

The $\mathcal{O}(\varepsilon^2)$ term in (27) can be calculated from (16) as

$$\frac{\partial\sigma}{\partial D}(k_c^2, D_c) = \frac{k_c^2(\Phi_\theta - G_0k_c^2)}{[\Phi_G + (D_c + 1)k_c^2 - \Gamma_G]G_0 - \Phi_\theta}. \tag{28}$$

Introduction of a slow time scale, $T = \varepsilon^2 t$, ensures that exponential growth terms, predicted by the linear analysis (15), can be written as $a(T)\exp(\pm ik_cx)$, where

$$a(T) = \exp\left(\frac{\partial\sigma}{\partial D}(k_c^2, D_c)\nu T\right), \tag{29}$$

and $\partial\sigma/\partial D(k_c^2, D_c)$ is given in (28).

With the new expressions for D (26) and T, we use (9)–(10) to write a vector equation for the perturbed system:

$$\mathbf{L}\begin{pmatrix}\theta-\theta_0\\ G-G_0\end{pmatrix}+\mathbf{N}+\mathbf{E}=\mathbf{0}, \tag{30}$$

where

$$\mathbf{L}=\begin{pmatrix}-G_0\dfrac{\partial^2}{\partial x^2}-\Phi_\theta & -\Phi_G\\ -\Gamma_\theta & -D_c\dfrac{\partial^2}{\partial x^2}-\Gamma_G\end{pmatrix}, \tag{31}$$

$$\mathbf{N}=\begin{pmatrix}-(G-G_0)\dfrac{\partial^2}{\partial x^2}(\theta-\theta_0)-\Phi_{\theta G}(\theta-\theta_0)(G-G_0)-\Phi_{\theta\theta}(\theta-\theta_0)^2/2\\ -\Phi_{\theta\theta G}(\theta-\theta_0)^2(G-G_0)/2-\Phi_{\theta\theta\theta}(\theta-\theta_0)^3/6\\ -\Gamma_{\theta G}(\theta-\theta_0)(G-G_0)-\Gamma_{\theta\theta}(\theta-\theta_0)^2/2\\ -\Gamma_{\theta\theta G}(\theta-\theta_0)^2(G-G_0)/2-\Gamma_{\theta\theta\theta}(\theta-\theta_0)^3/6\end{pmatrix}+\text{h.o.t.}, \tag{32}$$

$$\mathbf{E}=\varepsilon^2\begin{pmatrix}G_0\dfrac{\partial}{\partial T}(\theta-\theta_0)\\ G_0\dfrac{\partial}{\partial T}(\theta-\theta_0)+\dfrac{\partial}{\partial T}(G-G_0)-\nu\dfrac{\partial^2}{\partial x^2}(G-G_0)\end{pmatrix}+\text{h.o.t.}, \tag{33}$$

$$\Phi_G=\frac{\partial\Phi}{\partial G}(\theta_0,G_0)$$

and Φ_θ, $\Phi_{\theta G}$, $\Phi_{\theta\theta}$, $\Phi_{\theta\theta G}$, $\Phi_{\theta\theta\theta}$, Γ_θ, $\Gamma_{\theta G}$, $\Gamma_{\theta\theta}$, $\Gamma_{\theta\theta G}$ and $\Gamma_{\theta\theta\theta}$ are defined in a similar way to Φ_G, and h.o.t. indicates higher-order terms.

We assume asymptotic representations for θ and G, in the form

$$G=G_0+\sum_{j=1}\varepsilon^j G_j(x,T),\qquad \theta=\theta_0+\sum_{j=1}\varepsilon^j\theta_j(x,T). \tag{34}$$

Substitution into (30) results in a hierarchy of linear equations which are evaluated for increasing powers of ε.

The first such equation is

$$\mathbf{L}\begin{pmatrix}\theta_1\\ G_1\end{pmatrix}=\mathbf{0}, \tag{35}$$

while the equation for the j^{th} power of ε is

$$\mathbf{L}\begin{pmatrix}\theta_j\\ G_j\end{pmatrix}+\mathbf{N}_j+\mathbf{E}_j=\mathbf{0}, \tag{36}$$

where $\mathbf{N}_j$ and $\mathbf{E}_j$ are calculated from the terms $\theta_{j-1}, G_{j-1}, \ldots, \theta_1, G_1$. Since (35) possesses nontrivial solutions, a necessary and sufficient condition for a solution to

(36) is given by the orthogonality relation

$$\lim_{T\to\infty}\frac{1}{T}\int_0^T\int_0^{2\pi/k_c}(\theta^*, G^*)\cdot(\overline{\mathbf{N}_j+\mathbf{E}_j})\,dx\,dT = 0, \tag{37}$$

where $(\theta^*, G^*)^t$ is a bounded solution of the adjoint problem

$$\mathbf{L}^*\begin{pmatrix}\theta^*\\ G^*\end{pmatrix} = \mathbf{0},$$

and $\mathbf{L}^*$ is the adjoint of $\mathbf{L}$. This relation, given by the Fredholm Alternative, suppresses secular terms which arise if solutions to (35) are present in $\mathbf{N}_j + \mathbf{E}_j$.

Application of (37) to the hierarchy linear equations indicates that no secular terms arise in the first two powers of ε. The $\mathcal{O}(\varepsilon)$ solution is

$$\begin{pmatrix}\theta_1\\ G_1\end{pmatrix} = \mathbf{U}[a_1\cos(k_c x) + b_1\sin(k_c x)],$$

where $u_1 = 1$, $u_2 = \Gamma_\theta/(D_c k_c^2 - \Gamma_G)$, $a_1 = a_0 a(T)$, and $b_1 = b_0 a(T)$, and the constants a_0 and b_0 are determined by the boundary conditions. The $\mathcal{O}(\varepsilon^2)$ solution is

$$\begin{pmatrix}\theta_2\\ G_2\end{pmatrix} = \mathbf{U}[a_2\cos(k_c x) + b_2\sin(k_c x)]$$
$$+ \mathbf{V}^{(1)}\left[\left(\tfrac{a_1^2-b_1^2}{2}\right)\cos(2k_c x) + a_1 b_1\sin(2k_c x)\right] + \mathbf{V}^{(2)}\left(\tfrac{a_1^2+b_1^2}{2}\right), \tag{38}$$

where the complex forms for $v_1^{(1)}$, $v_2^{(1)}$, $v_1^{(2)}$, and $v_2^{(2)}$ are given in the appendix.

At $\mathcal{O}(\varepsilon^3)$ the orthogonality constraint (37) yields a Landau equation for the maximum amplitude $|\alpha|$ of θ_1, namely

$$\frac{1}{2}\frac{d}{dT}(a_1^2 + b_1^2) = \nu X(a_1^2 + b_1^2) - Y(a_1^2 + b_1^2)^2, \tag{39}$$

where

$$X = \frac{k_c^2(\Phi_\theta - G_0 k_c^2)}{[\Phi_G + (D_c+1)k_c^2 - \Gamma_G]G_0 - \Phi_\theta}, \tag{40}$$

[as predicted by (28) and (29)], and

$$\begin{aligned} Y = &\{2k_c^2 u_2 v_1^{(2)} + k_c^2(v_2^{(1)} + v_2^{(2)}/2) - \Phi_{\theta G}(u_2(v_1^{(1)} + v_1^{(2)}/2) + v_2^{(1)} + v_2^{(2)}/2)\\ &- \Phi_{\theta\theta}(v_1^{(1)} + v_1^{(2)}/2) - \Phi_{\theta\theta G}u_2/2 - \Phi_{\theta\theta\theta}/6 - [\Gamma_{\theta G}(u_2(v_1^{(1)} + v_1^{(2)}/2)\\ &+ v_2^{(1)} + v_2^{(2)}/2) - \Gamma_{\theta\theta}(v_1^{(1)} + v_1^{(2)}/2) - \Gamma_{\theta\theta G}u_2/2 - \Gamma_{\theta\theta\theta}/6]\\ &\times[\Phi_G/(D_c k_c^2 - \Gamma_G)]\}/\{2[G_0(1 + \Phi_G/(D_c k_c^2 - \Gamma_G)) + u_2\Phi_G/(D_c k_c^2 - \Gamma_G)]\} \end{aligned} \tag{41}$$

Periodic boundary conditions for G and θ mean that a_0 and b_0 are determined by Fourier series analysis of the initial infinitesimal perturbations about the steady state.

(Recall that $a_1 = a_0 a(T)$ and $b_1 = b_0 a(T)$.) Therefore, provided $\nu = +1$ and $Y > 0$, the Landau equation (39) predicts that the large time solution evolves to

$$\theta = \theta_0 + \varepsilon(X/Y)^{1/2} \sin(k_c(x + \alpha)) + \mathbb{O}(\varepsilon^2),$$

$$G = k_+(\theta_0)/k_-(\theta_0) + \varepsilon(X/Y)^{1/2} u_2 \sin(k_c(x + \alpha)) + \mathbb{O}(\varepsilon^2),$$

where $\theta_0 = (u_L - u_0)/L$ and $k_c\alpha = \tan^{-1}(a_0/b_0)$. Thus a_0 and b_0 only determine a shift in phase which does not affect the qualitative form of the solution when the boundary conditions are periodic.

3.1 Numerical Simulation of Stationary Pattern Formation

In the last section we showed that there is a bifurcation to the growth of unstable modes, of wavelength $2\pi/k_c$, as the gel-diffusion constant increases through a critical value, D_c. Provided the Landau constant, Y, is positive, these modes grow until the nonlinear and linear terms balance. In this section we numerically simulate the resulting stable pattern.

In preparation for the numerics, we give exact forms for (11) and (12) and show the resulting dispersion relation (16). We choose $k_+(\theta)$ and $k_-(\theta)$ as smooth functions given by

$$k_+(\theta) = k_1 + \frac{k_2 k_3 \theta^2}{1 + k_3\theta^2}, \tag{42}$$

$$k_-(\theta) = k_1 + \frac{k_2}{1 + k_3\theta^2}. \tag{43}$$

Thus $k_1 = k_+(0)$, $k_2 = k_-(0) - k_+(0)$, and k_3 scales the θ-dependencies for $k_+(\theta)$ and $k_-(\theta)$. Noting that $k_+(\theta) + k_-(\theta) = 2k_1 + k_2$, we observe that the θ-derivatives of $k_+(\theta)$ and $k_-(\theta)$ are equal in magnitude but opposite in sign. Using similar functions as Oster et al. (1985), we choose $\tau(\theta)$ and $\pi(\theta)$ as

$$\tau(\theta) = \frac{\tau}{1 + (\theta + \tau_1)^2}, \tag{44}$$

$$\pi(\theta) = \frac{\pi}{1 + \theta}. \tag{45}$$

Here τ and π are constants denoting the magnitudes of the $\tau(\theta)$ and $\pi(\theta)$, respectively, and $-\tau_1$ is the dilation at which the contractile elements are strongest.

Sample calculation parameters, which meet the constraints (20), (21), and (23), are chosen as

$$\Phi_\theta = 1, \quad \Phi_G = -3, \quad \Gamma_\theta = \frac{25}{12}, \quad \Gamma_G = -4, \quad G_0 = 2, \quad D_c = 32.$$

These are satisfied by

$$\theta_0 = 1, \quad \pi = 4, \quad \tau = 4, \quad \tau_1 = 0, \quad k_1 = 3.623, \quad k_2 = 4.754, \quad k_3 = 11.60 \tag{46}$$

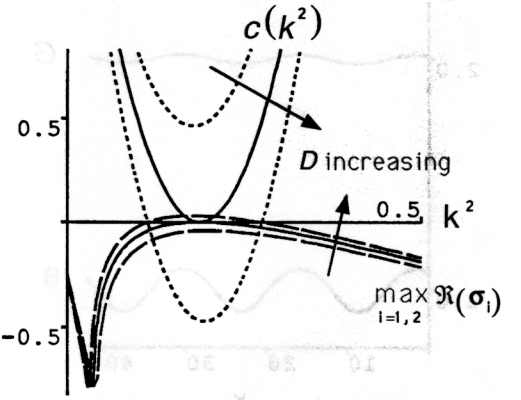

Fig. 3. The dispersion relation shows a critical bifurcation at $D = D_c$. The dispersion relation (16) is shown as D increases from $D = 28$ (subcritical, lower dashed line), through $D = D_c = 32$ (critical, solid line) to $D = 36$ (supercritical, upper dashed line). The quantity $c(k^2)$ is also shown for $D = 28$ (upper dotted line), $D = D_c = 32$ (solid line) and $D = 36$ (lower dotted line). The range of unstable modes (where $\max_{i=1,2} \Re(\sigma_i) > 0$) is given by $c(k^2) < 0$. Model parameter values are given in the text.

Thus (25), (40), and (41) give

$$k_c^2 = 0.1875, \quad u_2 = 0.2083, \quad X = 0.008762, \quad Y = 0.3821,$$

thereby indicating the potential for formation of stable patterns ($Y > 0$) which have a wave length of $2\pi/k_c = 14.51$. The resulting dispersion relation (16) goes through a critical bifurcation as D is increased through D_c. Figure 3 demonstrates this.

Using these parameter values and $D = 33$, a Crank-Nicholson-type finite difference scheme is used to numerically solve the model equations (9)–(10). Periodic boundary conditions for G and θ are used. Initial conditions are given by small (< 0.001) random perturbations of θ and G about their steady states (13). The resulting large-time solution is shown in Figure 4. By varying the set of random initial conditions, the numerical solutions shift to the right or left, although θ and G always remain in phase with each other (see Figure 4).

4. Two-dimensional Pattern-forming Capabilities

In this section we consider the two-dimensional pattern-forming capabilities of (1)–(2). We initially consider a simplification of the model which is valid for cytogels that have a very small shear modulus and whose viscous response is dominated by the energy dissipation which occurs during the sol-gel phase change. Experimental evidence supports this simplification: collagen gels are characterised by very high Poisson ratios (ν) (Oster et al., 1983). The Poisson ratio, given in terms of the bulk

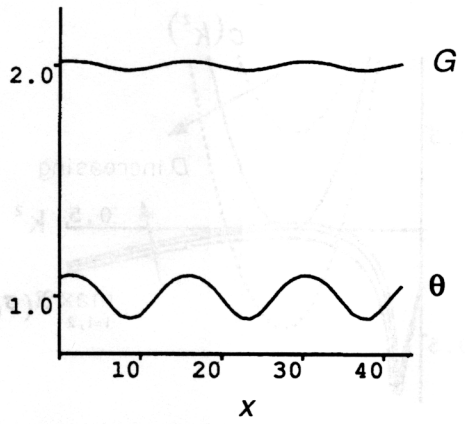

Fig. 4. Numerical solution of sol-gel equations. Shown is the large time ($t = 2000$), finite-difference, numerical solution of the model equations (9)–(10). Periodic boundary conditions for G and θ are used. Initial conditions are given by small (< 0.001) perturbations of θ and G about their steady states (13). Model parameter values are given in the text.

modulus K and the shear modulus g, is $\nu = (3K - 2g)/(6K + 2g)$, (Lur'e, 196 indicating that for these gels, the bulk modulus is far larger than the shear modulu Thus, the elastic response to stretching is characterised by bulk movements. We expe that the viscous stress term will be dominated by the energy dissipation which occu in the sol-gel phase change during bulk movements; because of the energy require to restructure the cross-linked cytogel in response to compression or dilation, the ne equilibrium is not found quickly. Hence, if the relaxation time for this process is lor compared to the time constant for the equilibration of shear stresses, the bulk viscosi μ_2 will dominate (see, for example, Landau and Lifshitz, 1979).

We show how the simplifying assumptions reduce the tensor force balance equatic (1) to a reaction-diffusion equation. Two-dimensional linear analysis of the resultir reaction-diffusion system shows analogous pattern-forming capabilities to those of th one-dimensional model, studied in Sections 2 and 3.

Analysis of the full, two-dimensional tensor equation model reveals that, when th shear modulus increases and becomes significant, requirements for a bifurcation spatial patterning become more stringent because the critical diffusion parameter als increases. If this critical diffusion coefficient is exceeded, an increased shear modulu means a longer wavelength for the resulting spatial pattern.

When the shear modulus (g) tends to zero, $E = 9gK/(3K + g)$ (Lur'e, 196 tends to zero and the Poisson ratio (ν) becomes $\frac{1}{2}$. Thus the constants $\gamma = E/(1 +$ and $1/\hat{\nu} = (1 - 2\nu)/\nu$ tend to zero and the product $\gamma\hat{\nu} = K$. We choose a nond mensionalization for (1)–(2) which remains valid as $g \to 0$, thereby adopting

form which has fewer parameters but which remains amenable to analysis:

$$G^* = \frac{G}{S_0}, \quad u^* = \frac{u}{\sqrt{\beta}}, \quad \hat{\nu}^* = \frac{\hat{\nu}}{\sqrt{\beta}}, \quad t^* = \frac{t\hat{\nu}\gamma}{\mu_2},$$

$$x^* = \frac{x}{\sqrt{\beta}}, \quad y^* = \frac{y}{\sqrt{\beta}}, \quad \pi^* = \frac{\pi c_0}{\hat{\nu}\gamma S_0}, \quad \tau^* = \frac{\tau}{\hat{\nu}\gamma},$$

$$\mu^* = \frac{\mu_1}{\mu_2}, \quad D^* = \frac{D_G \mu_2}{\hat{\nu}\gamma\beta}, \quad k_+^* = \frac{k_+\mu_2}{\hat{\nu}\gamma}, \quad k_-^* = \frac{k_-\mu_2}{\hat{\nu}\gamma}.$$

Again, dropping asterisks for notational simplicity, we write the nondimensionalized system as

$$\nabla \cdot \left\{ G\left[\mu\epsilon_t + \theta_t \mathbf{I} + (\epsilon - \Delta\epsilon)/\hat{\nu} + (\theta - \Delta\theta)\mathbf{I} + \tau(\theta)\mathbf{I}\right] - \pi(\theta)\mathbf{I} \right\} = 0, \quad (47)$$

$$\frac{\partial G}{\partial t} + \nabla \cdot \left(G \frac{\partial \mathbf{u}}{\partial t} \right) - D\Delta G - k_+(\theta) + k_-(\theta)G = 0. \quad (48)$$

4.1 Analysis of Model with Zero Shear Modulus

We consider a simplification of the model (47)–(48) which is valid for gels with a small shear modulus and a small ratio of shear viscosity to bulk viscosity. As described in the previous section, $\mu, 1/\hat{\nu} \to 0$. This simplifies (47) to

$$\nabla \cdot \left\{ G\left[\theta_t + \theta - \Delta\theta + \tau(\theta)\right] - \pi(\theta) \right\} \mathbf{I} = \mathbf{0}. \quad (49)$$

Assuming a constant time-independent boundary stress, σ_0 lets us integrate (49). We rewrite (49) and (48) as

$$G\frac{\partial \theta}{\partial t} - G\Delta\theta - \Phi(G, \theta) = 0, \quad (50)$$

$$\frac{\partial G}{\partial t} + \nabla \cdot \left(G \frac{\partial \mathbf{u}}{\partial t} \right) - D\Delta G - \Gamma(G, \theta) = 0, \quad (51)$$

where $\Phi(G, \theta)$ and $\Gamma(G, \theta)$ are given by (11) and (12). Thus the model is again simplified to a pair of reaction-diffusion equations which are two-dimensional analogues of (9) and (10).

As in the one-dimensional case, the steady state values for θ and G are given by (13). Linear analysis of (50) and (51) reveals an identical dispersion relation to that of the one-dimensional model (16). However, in this case, $k^2 = k_1^2 + k_2^2$, as the two-dimensional solutions to the linear system are of the form

$$\theta - \theta_0, \; G - G_0 \propto \exp[\sigma t + i(k_1 x + k_2 y)].$$

Thus, linear behavior of the two-dimensional reaction-diffusion model (50)–(51) is analogous to that of its one-dimensional version (9)–(10). We expect a similar bifurcation pattern formation, with a wave number k_c^2 (25), as D increases through D_c (24). In this case, however, two-dimensional spatial patterns result. These are numerically

simulated in Section 4.3. Before turning to these numerical simulations, however, we employ linear theory to suggest the possible spectrum of spatial patterns. In Section 4.2.2. we consider linear predictions for the geometry of patterns resulting from the general situation where there may be a non-zero shear modulus. The patterns which result as the shear modulus tends to zero are included within the context of this more general analysis.

4.2 Analysis of Model with Nonzero Shear Modulus

We now analyze the two-dimensional model (47)–(48), assuming that $1/\hat{\nu}$ and μ may be nonzero. Steady state values are given by

$$G = \frac{k_+(\theta_0)}{k_-(\theta_0)}, \quad \frac{\partial u}{\partial x} = \frac{\partial v}{\partial y} = \frac{\theta_0}{2}, \quad \frac{\partial v}{\partial x} = \frac{\partial u}{\partial y} = 0.$$

We assume that, at the steady state, there is a constant boundary stress, σ_0, so that θ_0 is given by

$$k_+(\theta_0)((1 + 1/(2\hat{\nu})\theta_0 + \tau(\theta_0))/k_-(\theta_0) - \pi(\theta_0) + \sigma_0 = 0. \tag{52}$$

To analyze the linear behavior of infinitesimal perturbations about the steady state, we require two state variables in addition to G. We choose θ and $\psi = \partial v/\partial x - \partial u/\partial y$; both of these are spatially homogeneous at the steady state ($\theta = \theta_0$ and $\psi = 0$) and invariant to rotations of the axes, reflecting the physical state of the system rather than the choice of coordinates.

We use the tensor identity

$$\nabla \cdot \boldsymbol{\epsilon} = \nabla\theta + \frac{1}{2}\begin{pmatrix} -\partial\psi/\partial y \\ \partial\psi/\partial x \end{pmatrix}$$

in writing the linearized system:

$$\begin{pmatrix} \frac{\partial}{\partial x}G_0\left[\frac{\partial}{\partial t} - \nabla^2 - \Phi_\theta/G_0 + \mu\frac{\partial}{\partial t} + (1-\nabla^2)/\hat{\nu}\right] & -\frac{\partial}{\partial y}G_0\left[\mu\frac{\partial}{\partial t} + (1-\nabla^2)/\hat{\nu}\right]/2 & \frac{\partial}{\partial x}[-\Phi_G + \theta_0/(2\hat{\nu})] \\ \frac{\partial}{\partial y}G_0\left[\frac{\partial}{\partial t} - \nabla^2 - \Phi_\theta/G_0 + \mu\frac{\partial}{\partial t} + (1-\nabla^2)/\hat{\nu}\right] & \frac{\partial}{\partial x}G_0\left[\mu\frac{\partial}{\partial t} + (1-\nabla^2)/\hat{\nu}\right]/2 & \frac{\partial}{\partial y}[-\Phi_G + \theta_0/(2\hat{\nu})] \\ G_0\frac{\partial}{\partial t} - \Gamma_\theta & 0 & \frac{\partial}{\partial t} - D\nabla^2 - \Gamma_G \end{pmatrix} \begin{pmatrix} \theta - \theta_0 \\ \psi - \psi_0 \\ G - G_0 \end{pmatrix} = \mathbf{0}, \tag{53}$$

where Φ_θ, Φ_G, Γ_θ, and Γ_G are as given for (14).

Looking for solutions of the form

$$\theta - \theta_0, \quad \psi - \psi_0, \quad G - G_0 \propto \exp[\sigma t + i(k_1 x + k_2 y)], \tag{54}$$

we determine the resulting dispersion relation to be

$$\frac{k^2}{2} G_0[\mu\sigma + (1 + k^2)/\hat{\nu}]\{G_0\sigma^2 + b(k^2)\sigma + c(k^2) + G_0[\mu\sigma + (1 + k^2)/\hat{\nu}](\sigma + Dk^2 - \Gamma_G) - (G_0\sigma - \Gamma_\theta)\theta_0/(2\hat{\nu})\} = 0. \tag{55}$$

where $b(k^2)$ and $c(k^2)$ are given by (17) and (18). Our previous analysis in Section 4.1 leads us to expect that when $\mu, 1/\hat{\nu} \to 0$, solutions to (55) coincide with those of (16). This is indeed the case.

4.2.1 Conditions for Bifurcation to Spatial Pattern. We now compare linear results from this model [(47)–(48)], which has a nonzero shear modulus, to those from the model of Section 4.1 [(50)–(51)], in which the shear modulus is zero. Following the procedure used in Section 3.1.1, we derive constraints for a bifurcation to spatial pattern and compare them to (20), (21), and (23). The resulting critical diffusion value D_{cr} is compared to the solution of (24).

The dispersion relation (55) is rewritten as

$$(1 + \mu)G_0\sigma^2 + b_1(k^2)\sigma + c_1(k^2) = 0, \tag{56}$$

where

$$b_1(k^2) = b(k^2) + G_0[\mu(Dk^2 - \Gamma_G) + (1 + k^2 - \theta_0/2)/\hat{\nu}], \tag{57}$$

$$c_1(k^2) = c(k^2) + G_0(1 + k^2)(Dk^2 - \Gamma_G)/\hat{\nu} + \Gamma_\theta\theta_0/(2\hat{\nu}) \tag{58}$$

$$= \alpha_1 k^4 - \beta_1 k^2 + \gamma_1,$$

for

$$\alpha_1 = G_0 D(1 + 1/\hat{\nu}), \tag{59}$$

$$\beta_1 = D(\Phi_\theta - G_0/\hat{\nu}) + G_0\Gamma_G(1 + 1/\hat{\nu}), \tag{60}$$

$$\gamma_1 = \Gamma_G(\Phi_\theta - G_0/\hat{\nu}) - \Gamma_\theta[\Phi_G - \theta_0/(2\hat{\nu})]. \tag{61}$$

Using identical arguments to those in Section 3.1.1, we write the conditions for stability when $k^2 \to 0^+$ as

$$b_1(0) = b(0) - G_0\mu\Gamma_G + (1 - \theta_0/2)/\hat{\nu} > 0, \tag{62}$$

$$c_1(0) = c(0) - G_0\Gamma_G/\hat{\nu} + \Gamma_\theta\theta_0/(2\hat{\nu}) > 0. \tag{63}$$

Provided that $\theta_0 \leq 2$, the constraints (62) and (63) are satisfied whenever (20) and (21) are met because $\Gamma_\theta > 0$ and $\Gamma_G < 0$ (see (12)).

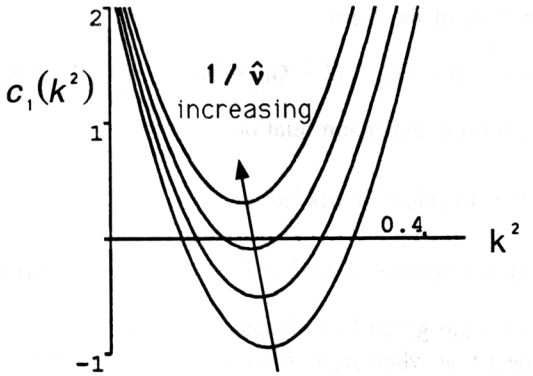

Fig. 5. Increasing the shear modulus decreases the range and magnitude of the unstable wave numbers. Unstable wave numbers are given by $c_1(k^2) < 0$. As $1/\hat{v}$ increases from 0 (lower graph) by increments of 0.015, the range and magnitude of these unstable wave numbers decreases until there are no unstable wave numbers for $1/\hat{v} = 0.045$ (upper graph). Parameter values are as given in Section 3.3, with $D = 40$.

Bifurcation to the growth of unstable modes occurs when $D = D_{cr}$ is the larger root of

$$[D(\Phi_\theta - G_0/\hat{v}) - G_0\Gamma_G(1 + 1/\hat{v})]^2 + 4\Gamma_\theta[\Phi_G - \theta_0/(2\hat{v})]G_0D(1 + 1/\hat{v}) = 0. \tag{64}$$

Comparison with (24) indicates that $D_{cr} > D_c$.

Provided that $D > D_{cr}$, unstable wave numbers k are given by $c_1(k^2) < 0$. We observe that, when the shear modulus increases, $1/\hat{v}$ increases and therefore the quantities $\beta_1/(2\alpha_1)$ and $(\sqrt{\beta_1^2 - 4\alpha_1\gamma_1})/(2\alpha_1)$ both decrease (see (58)). These reductions affect the range of unstable wave numbers. The former indicates that the range of unstable wave numbers is shifted to the left and the latter indicates that the size of the range is decreased (Figure 5). As shown in Figure 5, $D = 40$ goes from supercritical to subcritical as $1/\hat{v}$ increases from 0.030 to 0.045. Therefore the upper graph in Figure 5 has no unstable wave numbers [$c_1(k^2) > 0$ everywhere].

In summary, increasing the shear modulus raises the critical diffusion coefficient and thereby tends to stabilize the system. When this critical diffusion coefficient is exceeded, an increased shear modulus results in a longer wavelength for the resulting spatial pattern.

4.2.2 Linear Predictions for Spatial Patterns. Linear analysis [see (54)] predicts that as D increases through D_{cr} [see (64)], there is a supercritical bifurcation to the growth of unstable modes. These modes have a wavelength of $k^2 = k_{cr}^2 = k_{1c}^2 + k_{2c}^2$, which equals $\beta_1/(2\alpha_1)$ when $D = D_{cr}$ (see (58)). The spatial component of these modes is given by the time-independent eigenfunctions of (53). These eigenfunctions

have the form

$$\mathbf{U}\exp(k_{1c}x + k_{2c}y),$$

where $L_{k_{cr}}\mathbf{U} = 0$, and

$$L_k = \begin{pmatrix} -ik_1G_0[k^2 - \Phi_\theta/G_0 & ik_2G_0(1 & -k_1[-\Phi_G \\ +(1+k^2)/\hat{\nu}] & +k^2)/(2\hat{\nu}) & +\theta_0/(2\hat{\nu})] \\ -ik_2G_0[k^2 - \Phi_\theta/G_0 & -ik_1G_0(1 & -ik_2[-\Phi_G \\ +(1+k^2)/\hat{\nu}] & +k^2)/(2\hat{\nu}) & +\theta_0/(2\hat{\nu})] \\ -\Gamma_\theta & 0 & D_{cr}k^2 - \Gamma_G \end{pmatrix}, \tag{65}$$

arises from the action of the linear operator in (53) on terms of the form $\exp(k_1x + k_2y)$. This gives

$$\mathbf{U} = \begin{pmatrix} 1 \\ 0 \\ u_2 \end{pmatrix},$$

where

$$u_2 = \Gamma_\theta/(D_{cr}k_{cr}^2 - \Gamma_G). \tag{66}$$

From this analysis we expect that the unstable modes are *irrotational* ($\psi = 0$) and, as in the case when the shear modulus was zero, that the gel (G) and dilation (θ) fluctuations are in phase with each other ($u_2 > 0$).

When $D > D_{cr}$, the model is unstable ($\sigma(k^2) > 0$) for a range of wave numbers, $k_m^2 < k^2 < k_p^2$, where k_m^2 and k_p^2 are the smaller and larger roots of $c_1(k^2) = 0$ respectively [see (58)]. Application of zero-gradient boundary conditions at $x = y = 0$ constrains linear solutions to take the form

$$\begin{pmatrix} \theta - \theta_0 \\ \psi - \psi_0 \\ G - G_0 \end{pmatrix} \propto \mathbf{U}\exp(\sigma t)\cos(k_1x)\cos(k_2y). \tag{67}$$

Analysis of the potential patterns quickly becomes complicated; there is a multitude of wave number combinations where $k_1^2 + k_2^2 = k^2$, $k_m^2 < k^2 < k_p^2$, and by the principle of superposition, each of these may contribute to the perturbation in (67). However, domain geometry severely restricts the number of possibilities. For example, if the domain is rectangular, $0 \le x \le L_1$, $0 \le y \le L_2$, then the application of zero-gradient boundary conditions at $x = L_1$ and $y = L_2$ requires that

$$k_m^2 < \pi^2\left(\frac{n^2}{L_1^2} + \frac{m^2}{L_2^2}\right) < k_p^2$$

for integers n and m.

On nonrectangular domains, analysis can be far more complicated. We simplify the situation, however, by considering regular solutions for symmetric domains that tes-

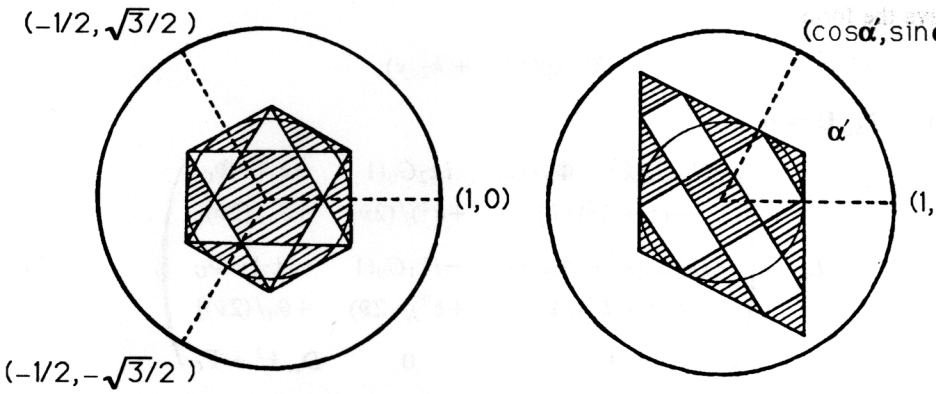

Fig. 6. Hexagonal and rhombic cell solutions tessellate the plane. The entire plane can be tile either of these elementary polygonal units. Each cell satisfies (67) with zero-gradient conditi on its boundary. Other solutions include square and roll cells (see text).

sellate the plane. This type of patterning is discussed in Murray and Oster (1984) a is briefly reviewed here (see also Murray (1989)). Patterns include squares, hexagon rhombi, and triangles. Thus the entire plane can be tiled by any one of these elementa polygonal units (or "cells"), which satisfy zero-gradient boundary conditions on the boundaries.

Square tessellation solutions are given by

$$\theta - \theta_0, \quad G - G_0 \propto \frac{1}{2}\left[\cos(k_{cr}x) + \cos(k_{cr}y)\right]. \tag{6}$$

This solution is invariant under a square rotation, in other words, a rotation of $\pi/$ radians.

The square cell solution is a special case of the rhombic solution (Figure 6) whic is given by

$$\theta - \theta_0, \quad G - G_0 \propto \frac{1}{2}\left\{\cos(k_{cr}x) + \cos[k_{cr}(x\cos(\alpha') + y\sin(\alpha'))]\right\}, \tag{6}$$

where α' is the rhombus angle. This solution is invariant under a rhombic rotatio in other words, a rotation of π radians. An illustrative pattern is shown in Figure The choice of $\alpha' = \pi/2$ yields (68).

The solution for a hexagon (Figure 6) is

$$\theta - \theta_0, \quad G - G_0 \propto \frac{1}{3}\left\{\cos[k_{cr}(-x/2 - \sqrt{3}y/2)]\right.$$

$$\left. + \cos[k_{cr}(-x/2 + \sqrt{3}y/2)] + \cos(k_{cr}x)\right\}. \tag{7}$$

This solution is invariant under a hexagonal rotation, in other words, a rotation $\pi/3$ radians. Again, Figure 6 illustrates this pattern. Triangles arise as subunits of th hexagonal pattern.

An additional cell-periodic solution is that of a one-dimensional roll pattern, given by

$$\theta - \theta_0, \quad G - G_0 \propto \cos(k_{cr} x). \tag{71}$$

In summary, possible linear growth patterns include those which tessellate the plane with square (68), rhombic (69), hexagonal (70), or roll (71) cells. These give some indication of the possible pattern diversity to expect when the full, nonlinear system is solved, but they by no means represent the total pattern formation potential.

4.3 Numerical Simulation of Model with Zero Shear Modulus

In the last section, we saw how domain geometry and boundary conditions play a crucial role in determining two-dimensional, patterned solutions to (47)–(48). We considered cell-periodic solutions which satisfied zero-gradient boundary conditions on their perimeter and tessellated the plane. However, exact numerical simulation of these cell-periodic solutions requires the application of zero-gradient boundary conditions on the perimeter of a domain which can contain a group of juxtapositioned cells. This poses no difficulty for square cells and rolls, but results in irregularly shaped domains for hexagonal and rhombic cells. For example, one cannot fit an exact number of hexagonal cells into a rectangular domain. Hexagonal and rhombic cells, however, yield repeating *rectangular* patterns, which satisfy *periodic*, rather than zero-gradient, boundary conditions on the perimeter of the rectangle.

In this section we discuss the numerical simulation of large-time solutions to equations (50)–(51). We use a Crank-Nicholson-type finite difference method and rectangular solution domains with periodic boundary conditions. These solutions indicate that the hexagonal pattern has a higher degree of structural stability than the square pattern.

Reaction kinetics are chosen which are identical to those used for the one-dimensional numerical simulation in Section 3.3. Thus $k_+(\theta)$, $k_-(\theta)$, $\tau(\theta)$, and $\pi(\theta)$ are given by (42), (43), (44), and (45) respectively. The sample calculation parameters are shown in (46). The critical diffusion coefficient, given by (24), is $D_c = 32$. The corresponding critical wave number k_c satisfies $k_c^2 = 0.1875$ (25). As a result of choosing $D = 34$, the range of unstable modes, given by $c(k^2) < 0$ [see (18) and Figure 3], is $0.1324 < k^2 < 0.25$.

We first consider a solution domain which supports *hexagonal* cells. Equation (70) indicates that hexagonal cells yield a repeating periodic pattern over the domain $0 \le x \le 4\pi/k_c$, $0 \le y \le 8\pi/(\sqrt{3}k_c)$. The model equations [(50)–(51)] were numerically solved over this domain for the parameter values described above. Boundary conditions were periodic, and initial conditions were given by small (< 0.001) random perturbations of θ and G about their steady states (13) (see Figure 7).

Equation (68) indicates that the solution domain, $0 \le x \le 4\pi/k_c$, $0 \le y \le 4\pi/k_c$, could support a repeating, periodic pattern of square cells. However, numerical simulations do *not* produce square cells; quasi-hexagonal patterns result (Figure 8). There are three major linear components to the solution, with angles $\pi - \alpha_0$, $\pi + \alpha_0$ and $3\pi/2$, where periodicity constraints gives $\alpha_0 = \tan^{-1}(1/2)$. This compares favorably with the measured angle of $\alpha_0 = 26.5$ degrees (0.463 radians) (Figure 8). The pattern would be truly hexagonal if α equaled $\pi/6 = 0.52$ radians.

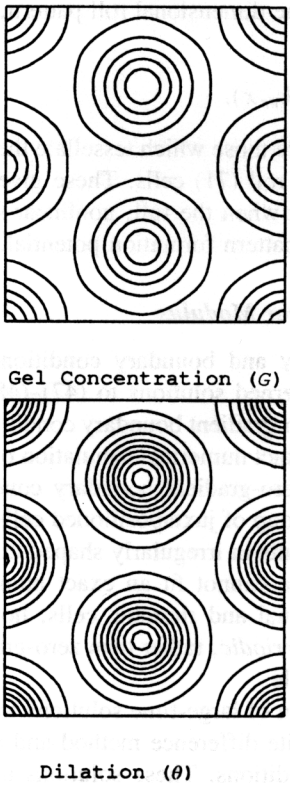

Fig. 7. Numerical solution yields hexagonal patterns. Shown is the large time ($t = 2000$), finite difference numerical solution of the model equations [(50)–(51)]. The domain size is given by $0 \leq x \leq 4\pi/k_c$, $0 \leq y \leq 8\pi/(\sqrt{3}k_c)$, where k_c and the model parameter values are given in the text. Boundary conditions are periodic and initial conditions are given by small (< 0.001) random perturbations of θ and G about their steady states.

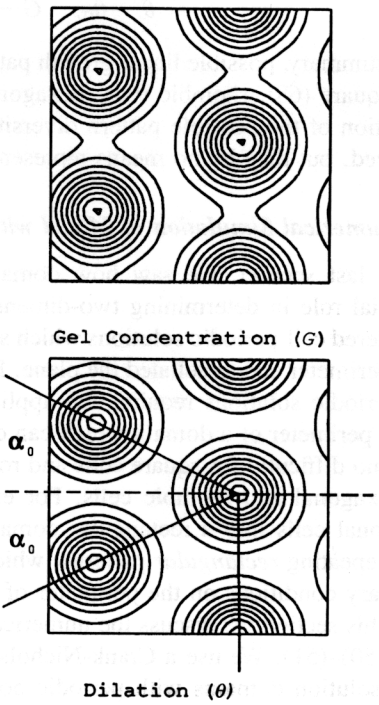

Fig. 8. Numerical solution yields quasi-hexagonal patterns. Shown is the large time ($t = 2000$), finite difference numerical solution of the model equations [(50)–(51)]. The domain size is given by $0 \leq x \leq 4\pi/k_c$, $0 \leq y \leq 4\pi/k_c$, where k_c and the model parameter values are given in the text. Boundary conditions are periodic and initial conditions are given by small (< 0.001) random perturbations of θ and G about their steady states. There are three major linear components to the solution, with angles $\pi - \alpha_0$, $\pi + \alpha_0$ and $3\pi/2$, where $\alpha = 26.5$ degrees.

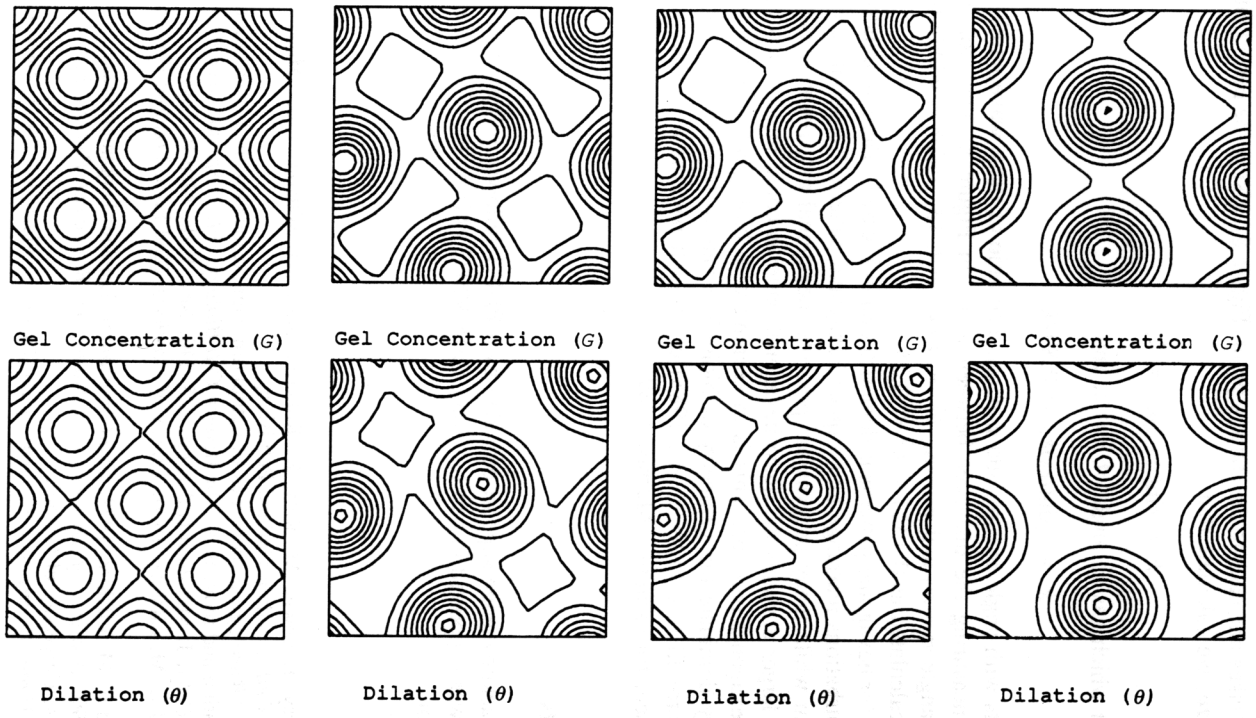

Fig. 9. Nonrandom "square cell" perturbations rearrange into a quasi-hexagonal pattern. Initial perturbations are given by (68), scaled so that the maximum perturbations for G and θ have magnitudes 0.025 and 0.125, respectively. Shown is the finite difference numerical solution of the model equations ((50)–(51)) for $t = 0$ (a), $t = 1500$ (b), $t = 3000$ (c) and $t = 4500$ (d). We see that by $t = 4500$ the initial square cell pattern has transformed into a quasi-hexagonal pattern. The domain size is given by $0 \leq x \leq 4\pi/k_c$, $0 \leq y \leq 4\pi/k_c$, where k_c and the model parameter values are given in the text. Boundary conditions are periodic.

The component which has an angle of $3\pi/2$ has a periodicity of two and the tw other components have a periodicity of four. In other words, moving through two four spatial cycles takes one back to the starting point (Figure 8). Using the periodici and the domain size, we calculate that

$$k = \sin(\pi/2)k_c = k_c$$

for the component which has an angle of $3\pi/2$, and

$$k = 2\sin(\alpha_0)k_c = 0.894k_c$$

for the components with angle $\pi - \alpha_0$ and $\pi + \alpha_0$. The ratio of these wave numbe is confirmed by measuring the distances between nodes in Figure 8. Thus for t components with angle $\pi - \alpha_0$ and $\pi + \alpha_0$, $k^2 = 0.8k_c^2 = 0.15$, which is within t range previously calculated as $0.1324 < k^2 < 0.25$.

The preference for hexagonal patterns is demonstrated in Figure 9. Here nonrando "square cell" perturbations rearrange into a quasi-hexagonal pattern. These numeric results suggest that while many patterns are possible, hexagonal patterns may occ preferentially. On larger domains the quasi-hexagonal patterns could more nearly a proximate truly hexagonal patterns. This is in keeping with biological observatior hexagons typically dominate the geometry of biological pattern formation, wheth giving rise to microvilli (see Oster et al., 1985) or to such patterns as feather a scale primordia (see, for example, Murray, 1989).

Acknowledgments

MAL would like acknowledge support provided by a PDF 1 fellowship from NSER of Canada. JDM was supported in part by Grant DMS-9003339 from the US Natior Science Foundation.

References

Alberts, B., D. Bray, J. Lewis, M. Raff, K. Roberts, and J. D. Watson. 1983. *Molecu Biology of the Cell*. London: Garland Publishing.

Condeelis, J. 1983. "Rheological properties of cytoplasm: significance for the organization spatial information and movement." In *Modern Cell Biology, Vol. 2: Spatial Organizati of Eucaryotic Cells*, J. McIntosh (Ed.), pp. 225–240. New York: Alan R. Liss.

Landau, L. D., and E. M. Lifshitz. 1970. *Theory of Elasticity*, (2nd Ed.). London: Pergam Press.

Landau, L. D., and E. M. Lifshitz. 1979. *Fluid Mechanics*. London: Pergamon Press.

Lewis, M. A. 1990. *Analysis of Dynamic and Stationary Biological Pattern Formati* D. Phil. Thesis, University of Oxford.

Lur'e, A. I. 1964. *Three-Dimensional Problems of the Theory of Elasticity*, Ch. 1. New Yo John Wiley.

Murray, J. D. 1989. *Mathematical Biology*. Heidelberg: Springer-Verlag.

Murray, J. D. and G. Oster 1984. "Generation of biological pattern and form." *J. Math. Ap Med. Biol.*, 1, 51–75.

Oster, G. F. 1984. "On the crawling of cells." *J. Embryol. Exp. Morph.*, 83, 329–364.

Oster, G. F., J. D. Murray, and A. K. Harris. 1983. "Mechanical aspects of mesenchymal morphogenesis." *J. Embryol. Exp. Morph.* 78, 83–125.

Oster, G. F., J. D. Murray, and G. M. Odell. 1985. "The formation of microvilli." In *Molecular Determinants of Animal Form*, G. M. Edelman (Ed.), pp. 365–384. New York: Alan R. Liss.

Oster, G. F., and G. M. Odell. 1984a. "Mechanics of cytogels I: Oscillations in *Physarum*." *Cell Motil.*, 4, 469–503.

Purcell, E. 1977. "Life at Low Reynolds Number." *Amer. J. Phys.*, 45, 1–11.

Taylor D., S. Hellewell, H. Virgin, and J. Heiple. 1979. "The solation-contraction coupling hypothesis of cell movements." In *Cell Motility*, S. Hatano (Ed.), pp. 363–377. Baltimore: University Park Press.

Appendix

Substitution of (34) into (30) results in a hierarchy of linear equations for increasing orders of ε. The solution to the $\mathcal{O}(\varepsilon^2)$ equation is given by (38) where

$$v_1^{(1)} = \frac{(-4D_c k_c^2 + \Gamma_G)(4u_2 k_c^2 - u_2\Phi_{\theta G} - \Phi_{\theta\theta}/2) + \Phi_G(u_2\Gamma_{\theta G} + \Gamma_{\theta\theta}/2)}{(4D_c k_c^2 - \Gamma_G)(4G_0 k_c^2 - \Phi_\theta) - \Phi_G\Gamma_\theta},$$

$$v_2^{(1)} = \frac{-\Gamma_\theta(4u_2 k_c^2 - u_2\Phi_{\theta G} - \Phi_{\theta\theta}/2) + (4G_0 k_c^2 - \Phi_\theta)(u_2\Gamma_{\theta G} + \Gamma_{\theta\theta}/2)}{(4D_c k_c^2 - \Gamma_G)(4G_0 k_c^2 - \Phi_\theta) - \Phi_G\Gamma_\theta},$$

$$v_1^{(2)} = \frac{-\Gamma_G(u_2\Phi_{\theta G} + \Phi_{\theta\theta}/2) + \Phi_G(u_2\Gamma_{\theta G} + \Gamma_{\theta\theta}/2)}{\Phi_\theta\Gamma_G - \Phi_G\Gamma_\theta},$$

$$v_2^{(2)} = \frac{\Gamma_\theta(u_2\Phi_{\theta G} + \Phi_{\theta\theta}/2) - \Phi_\theta(u_2\Gamma_{\theta G} + \Gamma_{\theta\theta}/2)}{\Phi_\theta\Gamma_G - \Phi_G\Gamma_\theta}.$$